fluids

MDPI

Article

Acceleration of Modeling Capability for GDI Spray by Machine-Learning Algorithms

Yassine El Marnissi [1], Kyungwon Lee [1] and Joonsik Hwang [1,2,3,*]

[1] Department of Mechanical Engineering, Mississippi State University, Starkville, MS 39762, USA; ye44@msstate.edu (Y.E.M.); kl1598@msstate.edu (K.L.)
[2] Center for Advanced Vehicular Systems (CAVS), Mississippi State University, Starkville, MS 39762, USA
[3] Institute for Clean Energy Technology (ICET), Mississippi State University, Starkville, MS 39762, USA
* Correspondence: hwang@me.msstate.edu

Abstract: Cold start causes a high amount of unburned hydrocarbon and particulate matter emissions in gasoline direct injection (GDI) engines. Therefore, it is necessary to understand the dynamics of spray during a cold start and develop a predictive model to form a better air-fuel mixture in the combustion chamber. In this study, an Artificial Neural Network (ANN) was designed to predict quantitative 3D liquid volume fraction, liquid penetration, and liquid width under different operating conditions. The model was trained with data derived from high-speed and Schlieren imaging experiments with a gasoline surrogate fuel, conducted in a constant volume spray vessel. A coolant circulator was used to simulate the low-temperature conditions (−7 °C) typical of cold starts. The results showed good agreement between machine learning predictions and experimental data, with an overall accuracy R^2 of 0.99 for predicting liquid penetration and liquid width. In addition, the developed ANN model was able to predict detailed dynamics of spray plumes. This confirms the robustness of the ANN in predicting spray characteristics and offers a promising tool to enhance GDI engine technologies.

Keywords: machine learning; Gasoline Direct Injection (GDI); projected liquid volume; tomographic reconstruction

Citation: El Marnissi, Y.; Lee, K.; Hwang, J. Acceleration of Modeling Capability for GDI Spray by Machine-Learning Algorithms. *Fluids* **2024**, *9*, 267. https://doi.org/10.3390/fluids9110267

Academic Editors: Filippos Sofos and N. Swaminathan

Received: 30 September 2024
Revised: 5 November 2024
Accepted: 15 November 2024
Published: 18 November 2024

1. Introduction

In recent decades, Gasoline engines has been recognized as one of the efficient and widely used internal combustion (IC) engines. Approximately 13 million gasoline cars were sold in the United States in 2023 [1]. However, it is important to note that Greenhouse gas emissions increased from 2022 to 2023 by 1.1 percent (36.8 billion Metric Tons) [2]. Gasoline direct injection (GDI) plays a significant role in contributing to these emissions and typically offers better fuel efficiency compared to Port Fuel Injection (PFI) engines [3]. Fuel is injected directly into the combustion chamber in GDI engines. This technique prevents wall wetting within the port, reduces the time required for fuel transport, provides precise regulation of fuel entering the combustion chamber, and has the potential for cleaner combustion. Multiple injections, along with high fuel injection pressure, improve control over the injection process, leading to a higher vaporization rate and thus overcoming cold start problems. Most of the technical challenges associated with conventional Port Fuel Injection (PFI) are overcome in GDI, particularly in achieving higher engine volumetric efficiencies. In GDI, the absence of vapor in the intake charge allows more air induction into the combustion chamber. Furthermore, the direct injection prevents engine knocking by using advanced evaporative cooling which lowers the in-cylinder temperature. However, GDI engines are facing challenges during start, which can lead to changes in the spray pattern and, consequently, delayed ignition. This delay can have an impact on the production of hydrocarbon (HC), carbon monoxide, and nitrogen oxide (NO_x). The spray break-up and mixing properties are affected by cold fuel temperature, which results in the

deterioration of the combustion process. One of the significant challenges to understanding the deterioration of the combustion process is the inappropriate injection parameter or undesired fuel properties. The analysis of spray evolution is notably complex due to the involvement of turbulent dispersed multiphase flows, as well as the injector design factors such as nozzle orifice, and the counterbore hole [4]. The spray formation and characteristics depend on the fuel properties and breakup, which are governed by the atmospheric, cold-start conditions. To address these challenges of spray behavior in the GDI engines, the adoption of machine learning could offer substantial improvement in predictive accuracy.

Literature on cold start spray pays attention to the examination of spray characteristics using non-invasive optical diagnostics [5,6]. The reliability of these optical diagnostic methods is crucial for acquiring experimental data, which forms the foundation for machine learning, particularly in training, and developing accurate and reliable predictive models of spray behavior. Tong et al. [7] focused on evaluating the impact of fuel volatility on the cold start performance of GDI engines using Planar Laser-Induced Fluorescence (PLIF) and Mie scattering. They found that during the initial phase of the cold start, low-volatility fuels result in unstable combustion and higher unburned hydrocarbon (UHC) emissions. Bruno et al. investigated the effects of injection pressures ranging from 2 MPa to 10 MPa on spray penetration and fuel distribution during cold starts using optical diagnostics. The experimental results indicated that degraded cold start performance was observed at pressures below 5 MPa, while the best performance was achieved at higher injection pressures combined with a late start of injection (SOI). Various optical diagnostics such as the Schlieren shadowgraph and high-speed imaging were utilized to examine the dispersion of liquid vapor and droplet atomization, providing detailed insights into spray dynamics and accurate data for training machine learning models.

Computational fluid dynamics (CFD) simulation also offers a detailed and cost-effective approach to understanding spray dynamics, designing new sprays, and optimizing device operating conditions. The predominant method to simulate sprays is the Lagrangian simulations [8]. Daniele [9] investigated the air-fuel mixing under a Spray G injector using a 3D CFD model. The simulation results agreed with the experimental measurements in terms of wall film formation and spray characteristics. Filippo et al. [10] studied the impact of the initial droplet distribution on the predicted spray physics using Lagrangian and Eulerian methods in liquid fuel atomization. They compared the results with the spray conditions of the baseline spray G from the ECN. The study found that accurate predictions of liquid and vapor penetration can be achieved through a careful selection of the initial mean droplet size, in conjunction with standard evaporation and breakup models. Despite the development of CFD, achieving precise details of spray evolution under cold start remains challenging due to complex spray dynamics associated with changes in fuel properties according to fuel and ambient temperatures.

Given this complexity, as simulations incorporate more complex phenomena, computational expenses rise. Selective use of machine learning offers a practical method to reduce computational costs [11,12]. To obtain more information on spray behavior and atomization, such as flow patterns, velocities, turbulence, and the breakup of liquid gasoline into smaller droplets, large datasets are necessary for CFD simulations. In contrast, machine learning can effectively predict both macroscopic and microscopic spray characteristics with only limited training data [13]. For a more in-depth insight into spray behavior, researchers commonly rely on Reynolds-Averaged Navier–Stokes (RANS). RANS averages flow properties over time to solve the governing equations for fluid flow and also provide a deeper understanding of the cold start behavior [14]. This detailed data from RANS simulations can serve as a useful foundation for supervised training in machine learning, which enhances its predictive capabilities in fluid dynamics [15]. Meanwhile the large eddy simulation (LES) approach seems to be better at predicting flow separation and is well-suited for unsteady or transient flows as it captures the large-scale turbulent structures [16]. Moreover, LES can be effectively combined with machine learning to enhance

simulations of spray phenomena and reduce memory occupation in overall combustion simulations [17,18].

Understanding the quantitative effects of various conditions on fuel spray behavior requires reliable experimental data that can serve as input to mathematical models capable of predicting fuel spray characteristics and spray dynamics. Recently, machine learning has become a viable approach to predict spray dynamics [19,20]. The continuous advancement of precise measurements and simulations is rapidly increasing the generation of vast amounts of data to cover a wide array of fields associated with classification, regression, and computer vision. The application of machine-learning algorithms to analyze extensive datasets is driving innovative advancements across a diverse range of fields. Nowadays, artificial neural network (ANN) models are used to investigate spray behavior in relation to various parameters, including nozzle design and engine-specific parameters. ANNs are employed due to their robust capacity for nonlinear fitting, with this fitting ability contingent upon the number of hidden layers, neurons, and hidden functions. Junjian [21] studied the spray tip penetration of octanol diesel by the ANN model. The study established 15 ANN models, and the results showed that models had a high prediction accuracy with an R^2 value of 0.99901, which was in good agreement with the experimental results of the 20% octanol-blended fuel. The use of ANN models allowed for better prediction results compared to existing mathematical models, avoiding prediction errors. The work of Hwang et al. [22] investigated the capability of a machine-learning algorithm to predict the spray morphology under ECN spray G conditions. They developed a predictive model based on a variant of linear regression and trained it using data from spray experiments carried out in a constant-flow spray vessel. The computed tomographic algorithm was used to construct a 3D spray from the projected liquid volume data at three viewing angles 0°, 11.25°, and 22.5°. The results from the predictive model showed excellent agreement with the experimental data, demonstrating the efficacy of linear regression with a set of nine input features to predict spray performance. Thangaraja [23] applied ANN to generate a wide range of thermophysical properties such as density, viscosity, specific heat, thermal conductivity, and more, for biodiesel fuels based on their composition and temperature. Following ANN applications, Seo et al. [24] estimated cold start emissions using an ANN. They developed various models that accurately predict the surge in carbon monoxide levels. Giannelli et al. [25] conducted an analysis of cold start emissions by using a series of Gaussian functions and a semi-empirical equation involving tractive power. The study considered the effect of catalyst warm-up and fast idle on emissions. Sabatini et al. [26] developed a semi-empirical temperature model to simulate thermal transients in a catalytic converter. They found that during the cold start, the model can estimate the high-off temperature.

In this study, the objective is to evaluate the capability of an ANN to accurately predict cold start spray dynamics and provide detailed quantitative information based on operational conditions such as fuel temperature and injection pressure. While previous studies have employed ANNs to model spray characteristics, a significant gap persists in developing models capable of accurately predicting the intricate 3D spray dynamics specific to cold-start conditions in GDI engines. By integrating data obtained from high-speed and Schlieren imaging into the ANN model, this research aims to develop a reliable tool that can predict 3D spray dynamics, liquid penetration, and liquid width. The predicted spray dynamics from the ANN model are compared with experimental data to ensure the model's validity. This tool is crucial for analyzing how the air-fuel mixture distribution behaves during the cold start of GDI engines, a key factor in reducing emissions and enhancing engine performance.

2. Experimental Setup

2.1. Injector Configuration and Test Fuel

The spray test was conducted under engine conditions in a constant volume vessel, controlled in pressure and temperature. A high-pressure GDI fuel injector is used to

inject fuel at seven different pressure levels, ranging from 50 bar to 350 bar. Its geometric parameters are listed in Table 1.

Table 1. Injector Nozzle Geometry.

Parameter	Specification
Nozzle type	Multi-hole nozzle
Number of Nozzles	8
Nozzle Shape	Axisymmetric
Nozzle Angle	26.6°
Inner Orifice Diameter	150.6 µm
Counter-bore Diameter	360.4 µm

The injector was preconditioned by circulating coolant to guarantee uniformity in the experiment. The fuel and injector temperature were measured using a 1/16 thermocouple. The lowest temperature reached by the injector tip was −7 °C. Despite efforts to lower it further, this was limited by the heat exchange with the coolant lines. A Teledyne ISCO 65X syringe pump (Teledyne labs, Mason, OH, USA) was used to generate the target fuel injection pressure.

A surrogate fuel designated as PACE-20 was used as the testing fuel due to its excellent performance in terms of RON, distillation curve evaluations, and its ability to accurately capture the realistic evaporative spray characteristics. Table 2 lists the properties of PACE-20 fuel.

Table 2. PACE-20 Fuel Properties.

	PACE-20
RON	92.1
MON	84.2
H:C	1.97
PMI	1.5
Ethanol [wt%]	10.2
Total Aromatics [wt%]	28.6
Total Olefins [wt%]	4.9
HOV [KJ/kg]	407.5
Density@ 15 °C [kg/L]	0.74

2.2. Optical Techniques

The experiments were carried out in a constant-volume vessel. Figure 1 represents the high-speed imaging setup. Schlieren imaging and high-speed extinction techniques are employed to capture the vapor and liquid phases, respectively. Two optical windows are specifically designated for these tasks. The high-speed visualization is achieved using five quartz windows, each having a diameter of 90 mm. The liquid phase spray is identified through diffused backlight illumination extinction imaging. A green LED with 60 ns TTL modulation is used to provide high visibility, paired with a Fresnel lens with a diameter and focal length of 150 mm each. The light is then directed through an engineered diffuser to evenly distribute it. To further enhance the accuracy and clarity of the image, we employ a band-pass filter with a bandwidth of 20 nm.

1. Top of Form

A Phantom (V611) camera (Vision Research Inc., Wayne, NJ, USA), renowned for its high-speed imaging capabilities, was utilized in this study. It was set with a higher shutter speed (14,000 fps) and a resolution of 608 × 608 pixels. For detailed imaging of the spray evolution, the camera was equipped with two lenses: an autofocus Nikkor lens with a 50 mm focal length and a wide maximum aperture of f/1.8.

The DBIE optical method was implemented to selectively capture the liquid phase (indicated by the green LED) and isolate it from the vapor phase. An injector with a rotating adapter was installed in the vessel chamber, enabling the adjustment of viewing angles in a clockwise direction at 0°, 11.25°, and 22.5°. These specific angles facilitate 3D tomographic reconstruction.

In this study, a Schlieren z-type configuration is employed for the visualization of vapor phases due to its high sensitivity to changes in the refractive index of air that occur when fuel vaporizes [27]. A red LED light is focused through a Nikkor lens and aperture. The light is then passed through a concave mirror that collimates the light and directs it through the test region. The light was then directed to a second concave mirror, which collects the parallel light rays. To enhance the sensitivity, a knife edge with a 50% cut-off at the focal point was used. The Schlieren and extinction imaging setups are identical and the components of the optical arrangement for the Schlieren setup are summarized in Table 3.

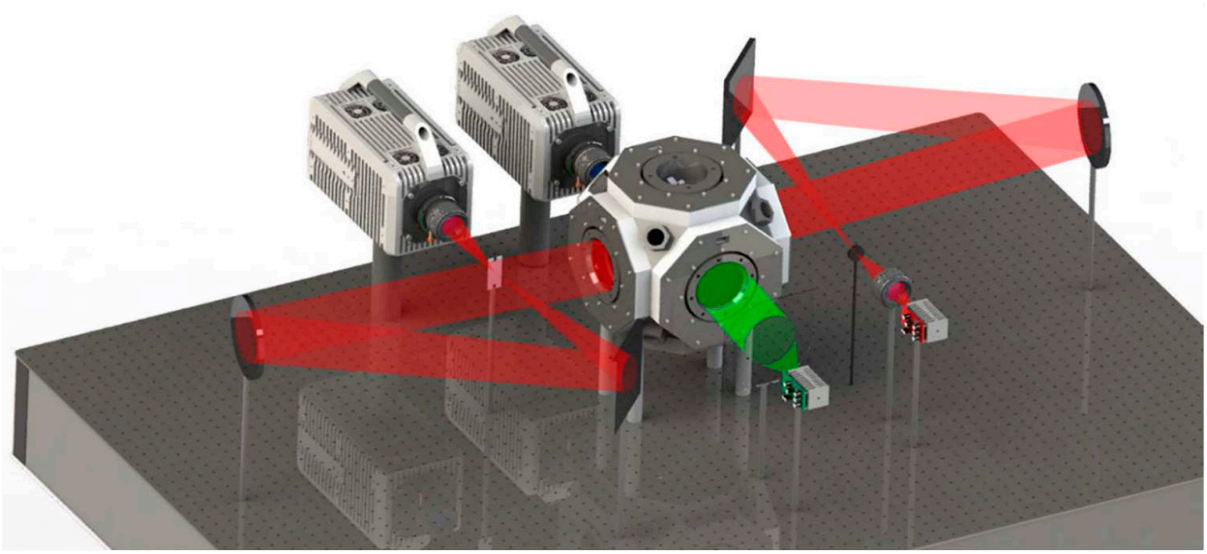

Figure 1. Experimental Setup for Extinction and Schlieren Imaging.

Table 3. Schlieren Optical Configuration Imaging Setup.

Component	Description
Camera and Lens	High-Speed Camera; Prime Lens: AF-S Nikkor 85 mm f/1.8G (Nikon)
Light Source and Lens	Red LED, 500 ns; Collection Lens: Nikkor, 50 mm f/1.8
Aperture and Collimation	0.5 mm diameter aperture; Collimating Mirror: GSO, 152 mm f/6.0 (Concave)
Light Path and Enhancement	Through spray region; Knife-Edge at focal point, ~50% cut-off

2.3. Schlieren Photography

In a Schlieren imaging setup, light travels uniformly through the spray test region. However, when it enters a medium with a different refractive index, the light rays are refracted. The corresponding linear relationship (Gladstone–Dale relation) relates the refractive index of the medium with the gas density [28]:

$$n - 1 = k\rho \tag{1}$$

where n represents the refractive index, ρ denotes the density, and k is the molar refractivity. Moreover, the change in the direction of a ray propagating in the z direction can be expressed as follows:

$$\varepsilon_x = \frac{L}{n_0}\frac{\partial n}{\partial x}\ \varepsilon_y = \frac{L}{n_0}\frac{\partial n}{\partial y}\ \text{Plane}\ (x - y) \tag{2}$$

where L and n_0 represent the optical distance and the index of refraction of the surroundings, respectively. Equations (1) and (2) demonstrate a clear correlation between the variations in the deflection angle and the gas density, which can be effectively captured through Schlieren imaging. Consequently, the deflection of light rays that pass through the spray region can be visualized and is dependent on the sensitivity of the Schlieren setup, resulting in an image with a distinctive background.

In order to isolate the spray region and remove background Schlieren fluctuation, an appropriate background intensity I_0 was subtracted from the spray image I. The detection of the vapor envelope was achieved using the "imgradient" function, which is available in the image-processing tool in MATLAB. Subsequently, an area detection method based on "bwperim" function was implemented. This function allows the identification of spray macroscopic characteristic parameters such as vapor penetration length which is defined as the distance between the nozzle tip and the furthest point on the vapor boundary at each injection. It is noteworthy that prior to using machine learning, the resultant images obtained by high-speed and Schlieren imaging might undergo preprocessing, including intensity normalization, noise reduction, and z-score normalization [29]. Such preprocessing is important for achieving accurate spray predictions [30].

3. Image Processing Technique

3.1. Extinction Imaging Method

Extinction imaging is a quantitative method for measuring liquid fuel concentration that provides more accurate measurements of spray characteristics compared to the standard Mie scattering method. The Mie scattering imaging technique is known to face challenges due to the inherent nature of its scattering process, which generates undesired signals in areas with dense particle concentrations. Consequently, extinction imaging is now recognized as a fundamental diagnostic technique in the field of spray research. The Projected Liquid Volume (PLV) along a defined line of sight is determined based on factors such as droplet size, the extinction coefficient, and liquid particle size. The formula to determine the optical thickness uses the Beer-Lambert law that relates the reduction in light intensity to the characteristics of the medium it passes through. The formula is defined as follows:

$$\tau = -\mathrm{In}\left(\frac{I}{I_0}\right) \tag{3}$$

where I and I_0 represent the transmitted and incident light intensities, respectively. This level of transmission is suitable for detecting the spray "edge" above the camera noise floor. However, it is important to take into account factors like vapor-phase beam steering. The optical depth, referred to as τ, is calculated and used to determine the Projected Liquid Volume (PLV). This suggests a spatial integration of the Liquid Volume Fraction (LVF) across the measurement domain, particularly in the cross-stream direction (y), as expressed in the following formula:

$$\mathrm{PLV} = \tau\frac{\pi d^3/6}{C_{ext}} = \int_{-y_\infty}^{y_\infty} (\mathrm{LVF}).dy \tag{4}$$

where d and C_{ext} are droplet diameter and extinction coefficient, respectively. The extinction coefficient (C_{ext}) represents the extent to which droplets in the medium attenuate light through absorption. Its value depends on the size of the droplets, the wavelength of light, the refractive index of the medium, and the collection angle of the optical setup. It was assumed, based on measurements taken during the injection across the plume, that the Sauter Mean Diameter (SMD) consistently approximated 12 µm. In addition, C_{ext} was determined to be 272×10^{-6} mm^2, based on a droplet diameter of 12 µm. This value was obtained for individual experimental setups using MiePlot v4.6 available at [31].

3.2. 3D Tomographic Reconstruction

The CT algorithm was used to construct a 3D spray from the liquid volume fraction (LVF) data at three different viewing angles 0°, 11.25°, and 22.5°. The reconstruction technique was carried out with MATLAB R2023b using a function like "iradon" for performing the inverse Radon transform and to support GPU computing. The reconstruction procedure was executed on axial sections extending from the nozzle tip to a position z = 60 mm downstream, with a hamming filter parameter value of 0.3. This approach offers detailed information about the distribution and movement of the plumes and better spatial and temporal resolution.

4. Machine Learning Method and Computational Framework

4.1. Machine Learning Networks

A multilayer feed-forward ANN has emerged as a modeling technique in predicting spray dynamics due to its high efficiency in identifying the nonlinear relationships between sets of input and output data. ANN accepts an input, propagates it through numerous layers of hidden neurons, and generates a prediction that links the input of all the neurons.

A neural network is essential because it involves adjusting the weights and biases of the neurons based on the input data. More specifically, Feed-forward ANN architecture comprises three types of layers: the input layer, the output layer, and hidden layers in between, as shown in Figure 2.

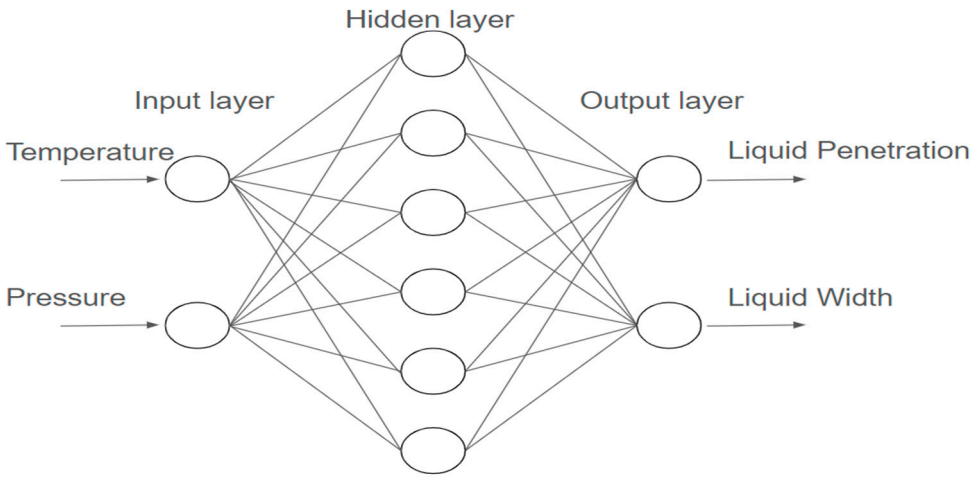

Figure 2. ANN structure with a single hidden layer.

An artificial neuron consists of numerous analog signal-processing elements known as "neurons". A neuron within the hidden layers can receive one or more input data $[X_1, X_2, \ldots, X_m]$. These inputs are transferred to the artificial neuron and subsequently multiplied by their respective synaptic weights W_i. An additional input signal, known as bias input w_0, is introduced to the artificial neuron alongside the input data. The neuron subsequently employs an activation function f(z), converts the weighted sum of input signals into output signals, and forwards the outcome to all the neurons in the subsequent layer.

$$y = f(z) = f\left(w_0 + \sum_{i=1}^{N} w_i x_i\right) \quad (5)$$

This process enables the network to learn from the data and enhances its ability to make accurate predictions and informed decisions.

There are different types of activation functions including linear, tangent, sigmoid, and hyperbolic. Among the mentioned functions, the sigmoid takes any real value as input and output values in the range 0 to 1.

In this paper, the sigmoid function is employed for all hidden layers and linear for the output layer, as it exhibits a satisfactory performance in terms of prediction. The coefficient

of determination and mean square error are taken as a valuable indicator of how well the input variables (injection pressure and fuel temperature) in our model explain the variations in the dependent variables, which is spray tip penetration.

The coefficient of determination and mean square error can be calculated as follows:

$$R^2 = 1 - \frac{\sum_{i=1}^{m}(Y_i - Y_{i,model})^2}{\sum_{i=1}^{m}(Y_i - \overline{Y}_i)^2} \quad (6)$$

$$MSE = \frac{1}{n}\left\{\left(Y_i - Y_{i,model}\right)^2\right\} \quad (7)$$

Y_i: The value of the variable to be predicted.
$Y_{i,model}$: Predicted value of Y_i.
$\overline{Y}_i$: The mean of the sample.
n: The number of values in the sample.

4.2. Computational Setup

Computational analyses were performed on a high-performance workstation equipped with an AMD Ryzen Threadripper 7980X (3.2 GHz, 64 cores), GeForce RTX 4090 24 GB GDDR6X, and 64 GB DDR5/6800MHz Kingston FURY Renegade memory, on a GIGABYTE TRX50 AERO D motherboard.

In this study, the projected liquid volume was measured through experiments and used as the target for the ANN. This ANN model is trained using input and target tables, which facilitates the management of extensive PLV data under various operational conditions. This approach enables the development of flexible networks that are optimized for efficient file size management, reduce storage demands, and improve computational efficiency while maintaining high accuracy. For training, we used two features—temperature and pressure—which served as inputs for the trained neural network. Each training step incorporates projected liquid volume (PLV) values obtained from experiments. It should also be noted that since our model is linear and does not contain complex terms such as products or power terms, we did not standardize these features.

For PACE-20 fuel, we predict LVF cold spray at -7 °C at pressures of 100 bar and 350 bar. Each condition, such as (-7 °C, 100 bar), is represented by a 1×300 cell array that captures the evolution of the spray. Within each cell of the array, there is a 608×608-pixel image of the spray, taken at distinct intervals within the 0 to 2 ms spray evolution.

4.3. Image Regression Modeling

In this study, the regression model for spray images of size ($M \times N$) was trained using temperature and pressure as input vectors, and the associated PLV data vector as the output. This study focuses on predicting the behavior of cold spray across a range of pressures and at various times. For each temperature, the ANN is trained using input tables paired with a range of injection pressures (50 bar to 350 bar). For the target, we organize the PLV data into 608 tables, each with dimensions of 608×7. We construct each table by extracting the first column from each set of PLV data images and placing it into the first of these 608 tables. We then proceed with the second column for the second table, and so forth. After assembling these tables, each one is trained individually. Once the ANN training is complete, we employ the reverse process, recompiling the trained columns back into 608×608 images. Figure 3 illustrates the schematic of the training algorithm for a spray image.

The mean processing time for the ANN to process seven images of specified size 608×608, corresponding to the seven pressures at a fixed temperature is 1 h. The training process involved 600 iterations and took nearly 3 h to predict three images from three different angles for PLV data (spray images). An early stopping mechanism was integrated to monitor validation performance. If the coefficient of determination (R^2) fell below 0.991 for any of the 608 tables, the training was stopped, and adjustments were made to the

number of neurons in the hidden layers until the model converged with an R^2 value greater than 0.991 before resuming the training process. The use of enhanced GPUs can accelerate this procedure. Model accuracy can be improved by optimizing the hidden layers or considering different activation functions. As shown in Figure 4, the ANN prediction accurately captures the overall shape and distribution of the spray core region. However, at the edges, there is a presence of minor noise, which may be attributed to the variability in pixel intensities resulting from the optical techniques used during the experimental image acquisition.

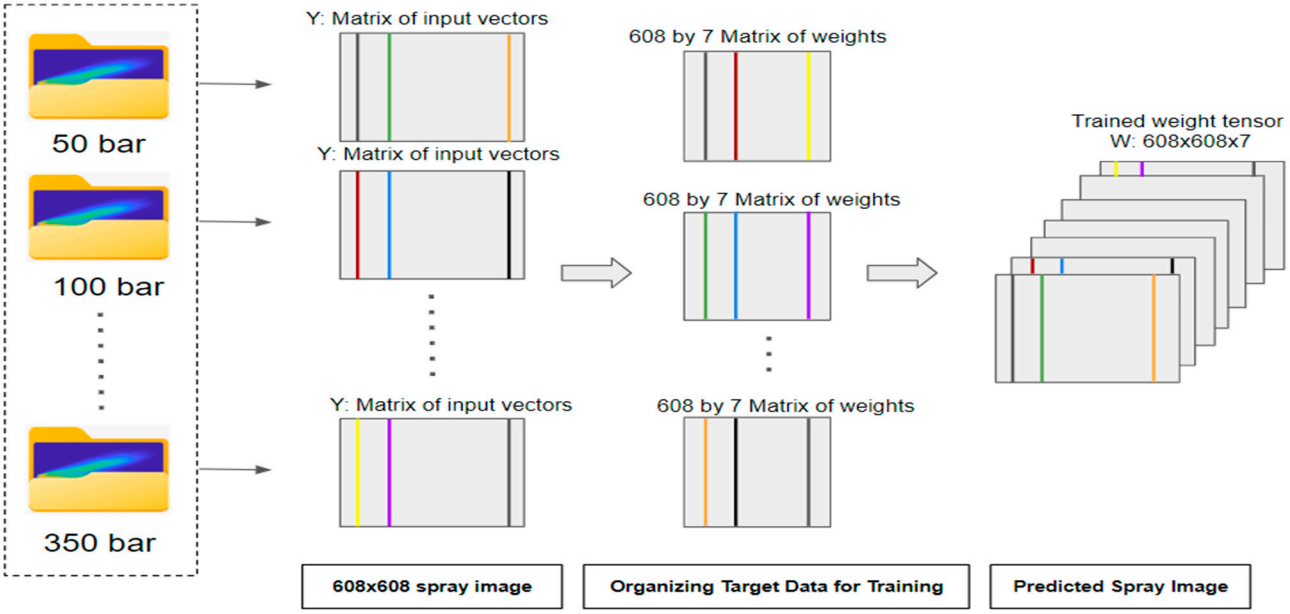

Figure 3. ANN Training Framework for Spray Topology Reconstruction.

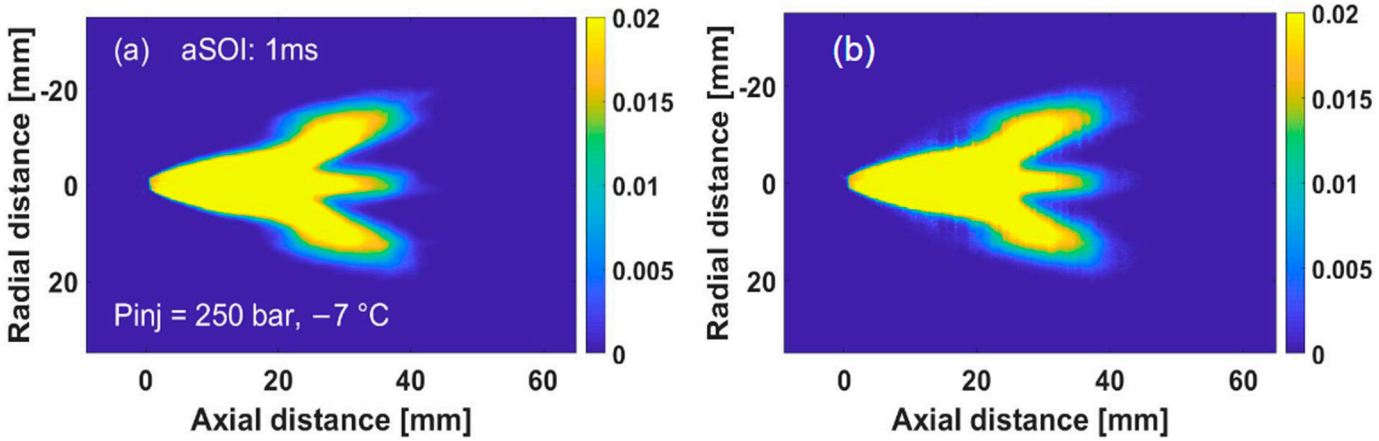

Figure 4. (**a**) Experimental PLV Map. (**b**) PLV Map Predicted by ANN (Machine Learning).

The trained regression model predicts the spray dynamics at any time step, thanks to the strategy of training a time series regression model and methodically repeating this process. This offers a significant advantage compared to CFD models that require time-stepping simulations. The ANN enables rapid optimization of complex processes, which allows for quicker adjustments with fewer simulations for more efficient outcomes [32]. It should also be noted that recent studies have developed a hybrid method combining machine learning (ML) and numerical methods. This approach aims to address errors in under-resolved simulations and reduce computational time. Dmitrii et al. [33] introduced a new approach for solving nonlinear partial differential equations. In this study, ML is

employed to enhance the approximations within CFD simulations and provide accurate solutions at each point on a grid that would be considered too coarse to accurately resolve the dynamics.

5. Results and Discussion

5.1. Experimental and Machine Learning Prediction of Liquid and Vapor Spray

The liquid penetration and liquid width significantly influence the spray morphology. Accordingly, the line-of-sight data analysis was performed using a PLV threshold of 0.2×10^3 mm^3 (liquid)/mm^2. The PLV data represents the average of 20 experimental runs under each set of working conditions. To ensure reliability, we used the mean standard errors of both liquid penetration and width, denoted as SEM = $\sigma/\sqrt{n}$ values. These mean standard errors were found too small to be discernible in the figures. Measurements of liquid penetration length and liquid width were obtained under different injection pressure conditions P_{inj} = [50, 150, 350] bar and T_{fuel} = [−7, 60] °C. Figure 5 illustrates the temporal evolution of PLV and Schlieren patterns captured at the initial stages of spray formation under 50 bar and −7 °C. Both liquid penetration and liquid width were synchronized at the time just after the actual start of injection. The experimental images that were acquired indicated the presence of an injection delay, characterized as the time between the start of electronic command and the start of injection (SOI). As a result, it was observed that the early spray formation for the hot fuel was faster in comparison to the cold fuel scenarios due to the reduced viscosity of the hot fuel, which allows fast needle opening. In addition, hot fuel spray promotes better atomization and faster spray formation from multi-hole injectors [34]. Meanwhile, the cold fuel spray affects stability due to the straighter edges produced, which indicate weaker vortex formation and reduced mixing with air [35]. The results showed that as injection pressure increases, both liquid and vapor penetration lengthen due to enhanced air entrainment and increased flow momentum. It is also observed that the liquid penetration initially increases linearly during the first phase, which includes acceleration and the first transition stages, followed by the quasi-steady stage and second transition, where the penetration reaches its maximum and subsequently becomes stagnant.

By comparing the liquid and vapor penetration at high and low temperatures, it can be observed that with an increase in injection pressure, the liquid/vapor at high temperatures extends further in comparison to low temperatures [36]. At high injection pressure, a significant difference in liquid width was observed between the distances of 15 mm and 30 mm. Furthermore, in the PLV and Schlieren intermittency images at high temperatures, the spray encountered collapsing, resulting in an accelerated axial penetration of liquid/vapor due to spray momentum. Based on these, detailed experimental data and insights serve as the foundation of the ANN model to predict the dynamics of spray under various operational conditions.

It is widely agreed that factors such as injection pressure and fuel temperature affect spray penetration and width. However, it is evidently impractical to account for every factor in the development of an ANN model. The objective of our model is not to create a general model encompassing liquid penetration and width under various conditions, but rather to specifically provide quantitative information on the effects of injection and environmental conditions on the behavior of the spray. With a focus on liquid penetration, width, and 3D LVF predictions under cold-start conditions using the ML algorithm, successful predictions in this domain are expected to be applicable to vapor spray behaviors as well. The PLV dataset resulting from these experiments was used to train an ANN model that predicts the spray under various operational conditions P_{inj} = [50, 150, 350] bar and T_{fuel} = [−7, 60] °C. It is worth noting that the modeling approach is designed to achieve high accuracy. A series of tests conducted on various ANN architectures revealed that a configuration with two layers was particularly effective in accurately predicting the spray image. Table 4 illustrates the ANN architecture, comprising an input layer with two neurons, a hidden layer with two neurons, and an output layer with a variable neuron. The training of the ANN is performed

using the Levenberg-Marquardt training algorithms available within the MATLAB Neural Fitting Tool (nftool). The choice of the best ANN network is based on the coefficient of determination R^2-values for training, validation, and testing. The model is developed using experimental data from PACE-20. In this process, 70% of the data is randomly selected for the training set, while 15% is randomly chosen for both testing and validation. The ANN training process for predicting spray characteristics (liquid penetration and width) involved 200 iterations, and it took less than 1 min to complete.

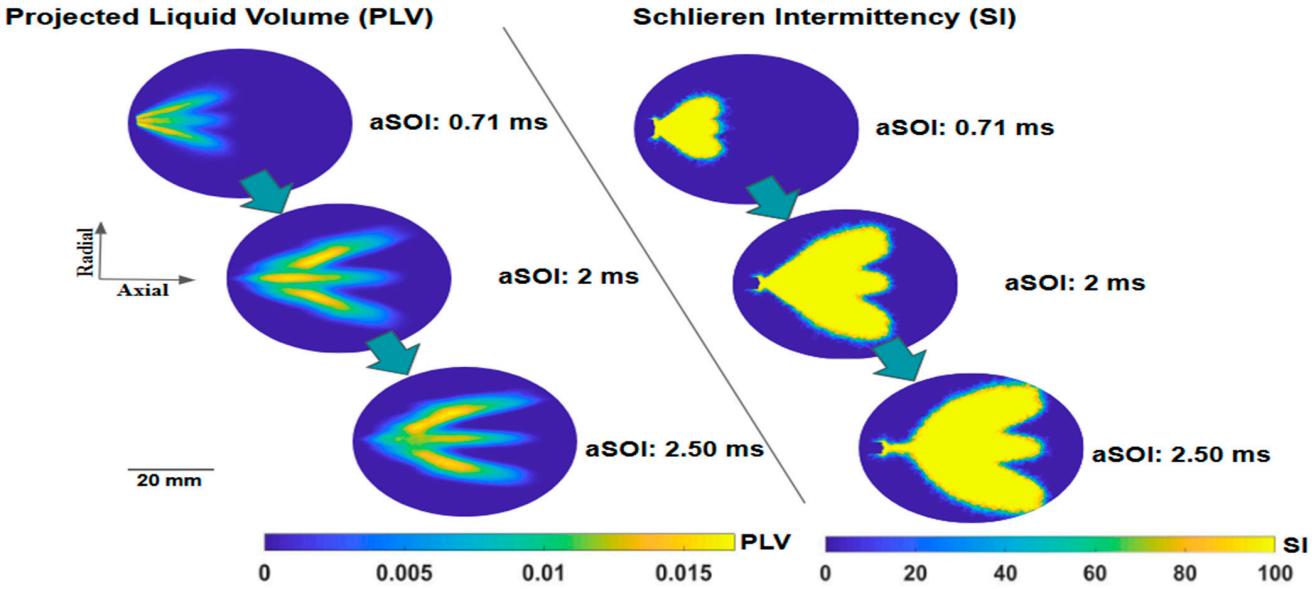

Figure 5. Temporal Evolution of PLV and Schlieren Patterns Under 50 bar and −7 °C.

Table 4. ANN configuration.

Criteria	Details
Image dimensions	608 × 608
Data input	7 PLV values (images of spray)
Feature set	2 characteristics: Fuel temperature (°C) and injection pressure (bar)
ANN Architecture	Input layer 2 × hidden layer 2
Training Algorithm function	Levenberg Marquardt
Training Data Points (70%)	PLV (−7 °C): 209,093 Liquid Penetration and Width: 2940
Validation Data Points (15%)	PLV (−7 °C): 44,806 Liquid Penetration and Width: 630

Figure 6 illustrates the temporal evolution of liquid penetration and width over time after the start of injection (aSOI) at these conditions. Solid lines are true values from experiments and symbols are predicted by the machine learning model. In the analysis of liquid penetration and width, the results indicate that the largest deviations between the predicted values by the ANN and the experimental data for both the liquid length and liquid width throughout the injection phase are 3.1 mm with an error of 5.16%, and 0.9 mm with an error of 3.10%, respectively. Similarly, as observed, the developed model accurately predicts the vapor penetration length and vapor width, with small deviations between the experimental and predicted results, showing an error of just 0.7%. Moreover, predicting spray behavior using CFD under various conditions, such as cold starts and hot fuel scenarios, can be challenging due to complex physical processes that include spray dynamics, the effects of temperature and pressure variations, and droplet behavior affected by air entrainment, which increases the turbulence of spray motion [37]. In contrast, the

developed machine learning model has shown good agreement with the experimental data in accurately predicting the penetration and width of both liquid and vapor. It is noteworthy that the results indicate a reasonably strong fit for all datasets that include both liquid and vapor spray, with an overall R^2 of more than 0.99. Figure 7 illustrates the training accuracy of the ANN model in predicting liquid penetration.

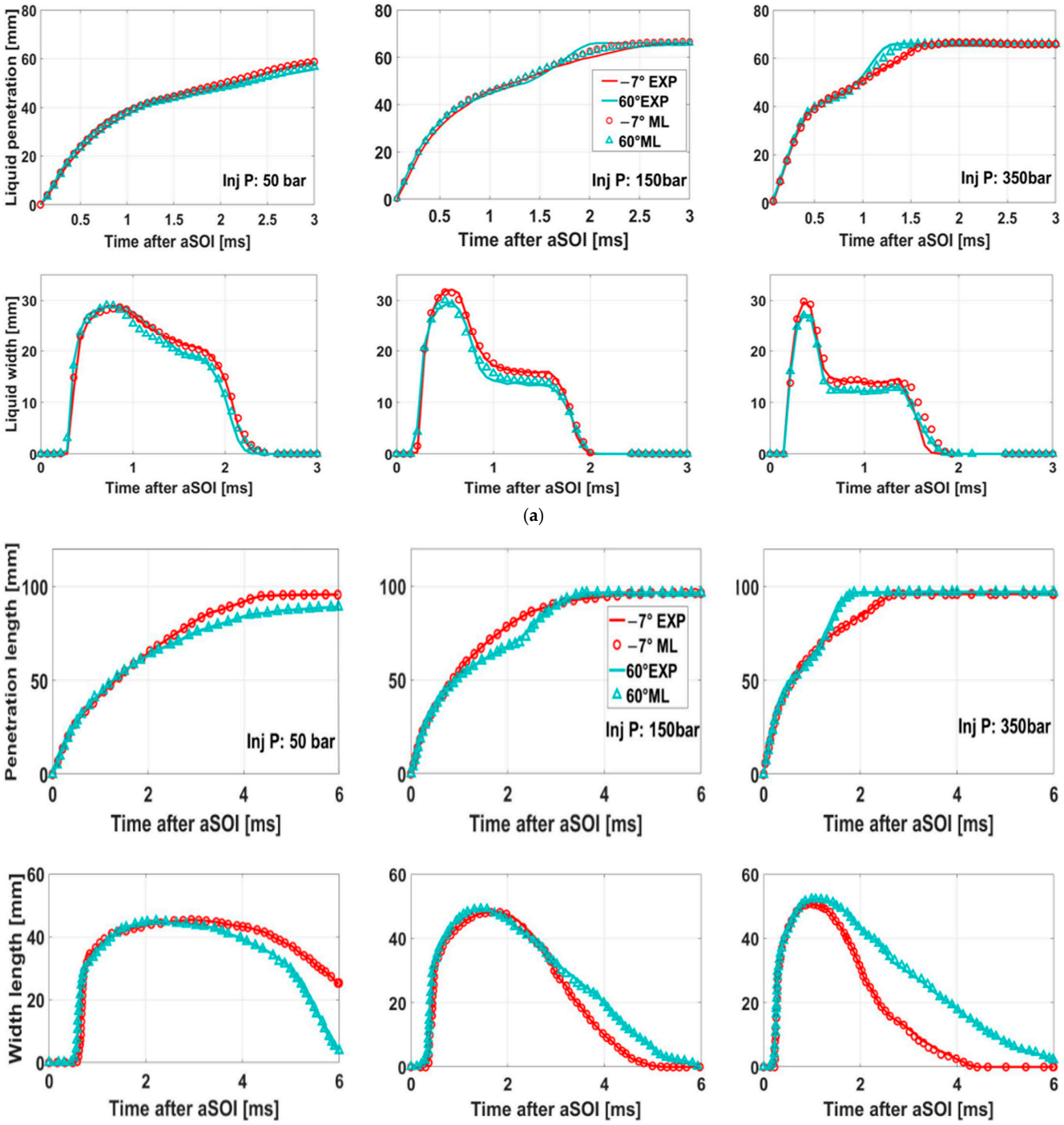

Figure 6. Analysis of Penetration and Width: Experimental and ANN-Predicted Values. (**a**) liquid penetration; liquid width @ 15 mm (**b**) vapor penetration; vapor width @ 30 mm.

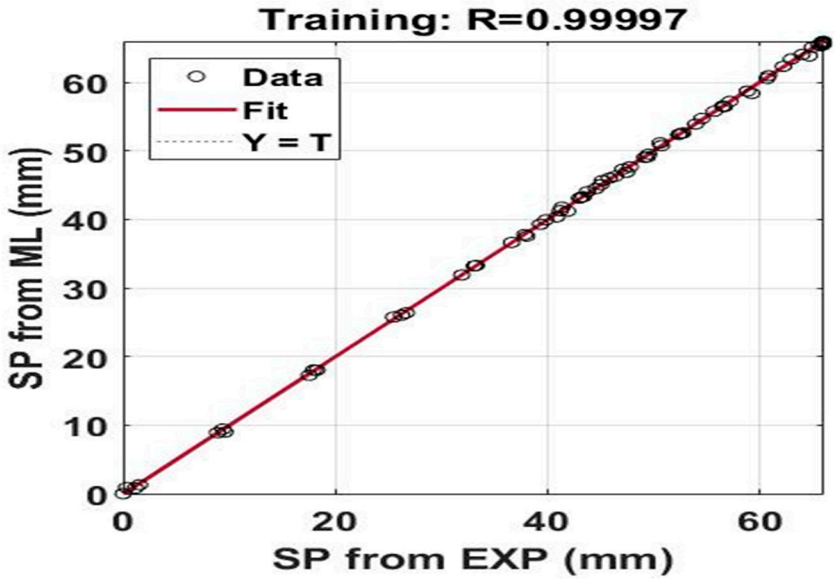

Figure 7. ANN Training Regression Plot for Spray Penetration (SP) Prediction.

5.2. Liquid Volume Fraction Prediction and Validation

The spatio-temporal evolution of the spray is displayed in Figure 8. Several interesting findings arise from the 3D liquid volume fraction (LVF). Notably, it is observed that at higher fuel temperatures and injection pressure, the spray morphology exhibits a strong plume collapsing toward the core area of the spray. The variation in fuel plume shape is influenced by the number of injector holes and their length-to-diameter (L/D) ratios. As the number of holes in the injector increases, the fuel plume broadens, leading to a larger collapse length. It should be noted that at higher injection pressures, the fuel plumes ejected from the orifices may interact with each other. This trend is clearly noticeable in 3D LVF at 350 bar. The collapsed spray then merges and forms a continuous closed region that blocks ambient gas from entering the central region. This leads to a decrease in pressure within the central area as the spray moves downward. The collapse of the plume can be attributed to an increase in the plume cone angle or a deviation in the plume direction from the injector axis. The edges of the plume cones overlap, leading to an increase in velocity at the intersection of the plumes. Then, the plumes start to merge into a single formation, which is characterized by a single velocity peak. It is important to emphasize that with an increase in ambient density, the central recirculation zone disappears, leading to a collapse of the plumes. More specifically, when the plumes are injected into a denser environment, the spray penetration tends to decrease. The ANN model is expected to replicate these observations, showing its potential to accurately predict complex fluid dynamics.

In this study, we used a MATLAB code enhanced for GPU processing to process and reconstruct three-dimensional spray dynamics from ANN-predicted images at different angles of 0°, 11.25°, and 22.5°, as illustrated in Figure 9. It should be noted that the predicted images from these three angles contained slight noise, which affected the clarity and intensity consistency. The source of this issue is the light source in the imaging experimental setup, which does not emit light uniformly but rather radiates over a range of angles due to diffuse radiation. This impacts the accuracy of quantifying the liquid phase in the spray during the experiment and consequently affects the predicted images, which may not accurately reflect the edges of the liquid phase [38]. To mitigate this issue, we applied a noise reduction technique using the 'imfilter' function. This algorithm efficiently handled large 608 × 608-pixel image datasets. Through advanced filtering, weighted sums, and symmetry operations, the code assembled cross-sectional planes from these predicted images, which enabled the creation of detailed 3D visualizations from 2D views. The resulting figure shows a 3D spray prediction at 100 bar, −7 °C, and 350 bar, −7 °C, captured at aSOI 1.14 ms and 1.87 ms, respectively. This innovative approach, which

combines ANN-based image prediction with advanced 3D spray reconstruction, represents a valuable step in the field of fluid dynamics research. It is important to note that the 3D spray distribution offers quantitative insights into the temporal evolution of both cold and hot fuel spray behaviors, and such LVF data serves to validate and refine CFD models. It was observed that at higher injection pressure and fuel temperature, plume collapsing becomes more prominent. This phenomenon is characterized by a strong plume movement towards the core area. The results, as shown in Figure 10, show a strong agreement between the experimental data and the spray behavior predicted by the model. The model successfully captures the complete plume dynamics, with distinct plumes at low pressure and plumes collapsing at high pressure.

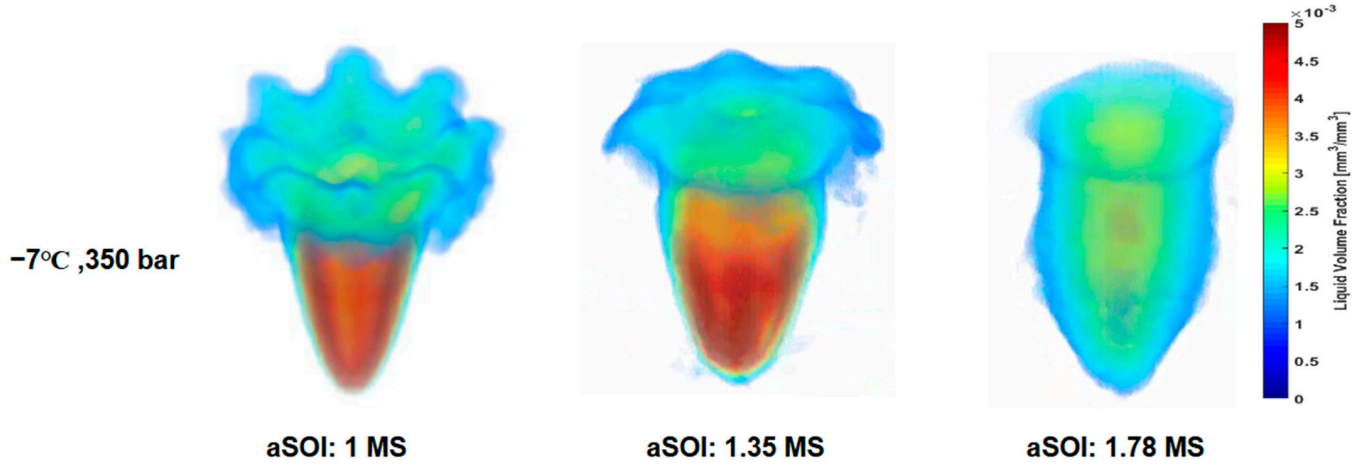

Figure 8. Temporal Evolution of 3D LVF during Cold Start.

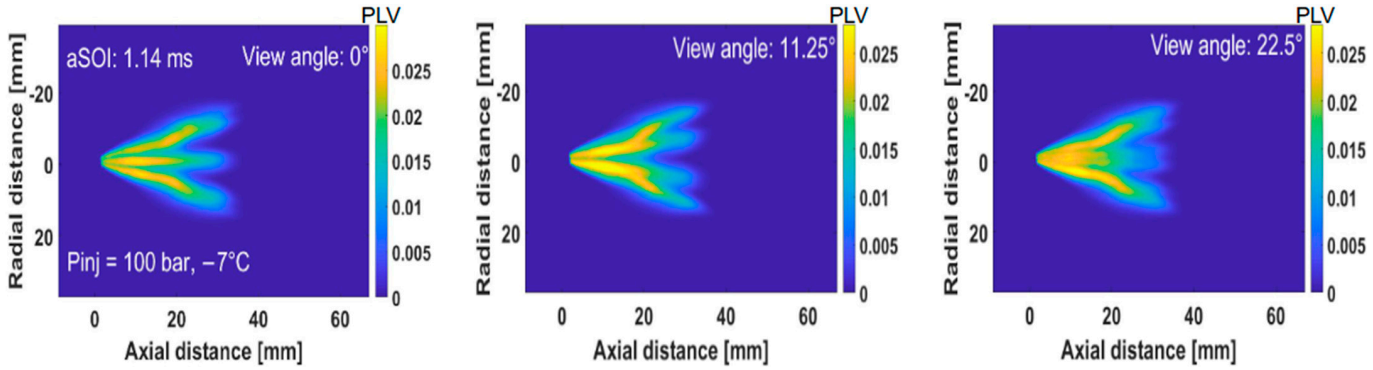

Figure 9. ML predicted spray images at (−7 °C, 100 bar), 1.14ms: Angles 0°, 11.25°, and 22.5°.

To summarize, ANN spray analysis is a powerful algorithm used to predict spray morphology and serves as an effective intermediate tool. However, it does not completely substitute for CFD simulations because its performance depends on the training data used to modify the neuron weights. For data that falls outside the target dataset, its accuracy may not be reliable. A trained ANN can serve as a useful bridge between experiments and CFD simulations. It can enhance the understanding of plume dynamics and offer validation for CFD simulation results in cases where experimental data is unavailable. Additionally, it can improve CFD simulations by providing valuable initial data.

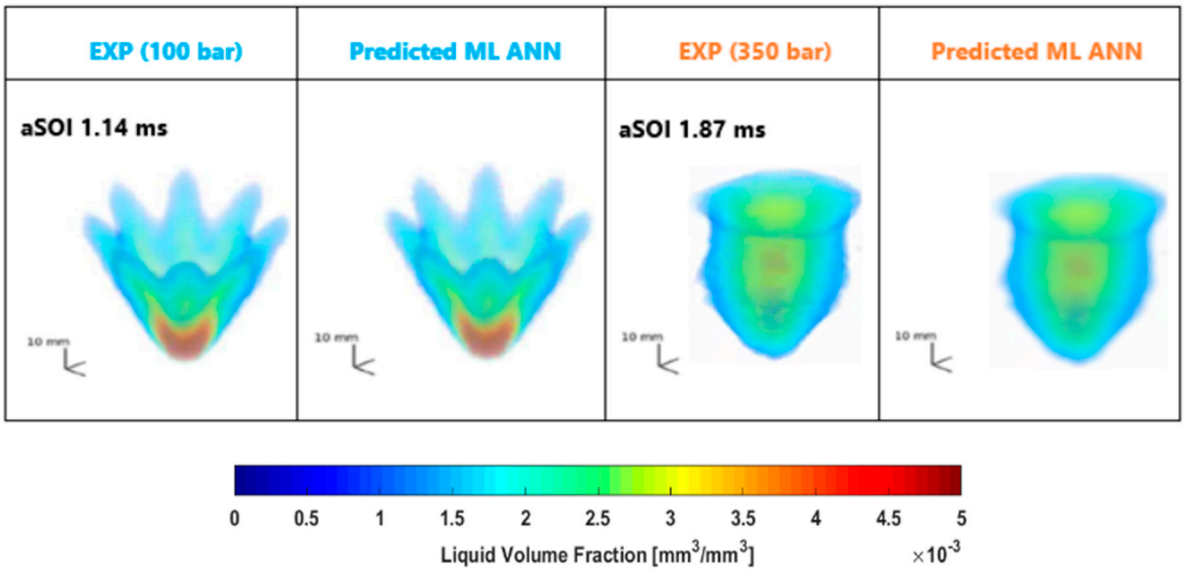

Figure 10. Experimental and ANN Prediction of 3D LVF Distribution.

6. Conclusions

In this study, a machine learning technique was implemented to predict the gasoline spray morphology under various injection pressures and fuel temperatures. A set of experimental datasets obtained from various optical diagnostic techniques, such as high-speed and Schlieren imaging, was utilized to train and validate the ANN model. The developed machine-learning algorithm was adept at predicting line-of-sight measurements and 3D liquid volume, providing quantitative information about 3D spray through the computed tomography (CT) algorithm. This approach might provide additional insight into future studies and can be adapted for models that predict both cold-start spray dynamics and hot fuel spray.

The main conclusions of this study are as follows:

1. The developed ANN predicts the liquid/vapor penetration length and width with high accuracy ($R^2 > 0.99$), showing strong agreement with experimental results.
2. The ANN model accurately predicts plume behavior that captures distinct plumes at low injection pressure (100 bar) and their collapse at high injection pressure (350 bar) which is still challenging for CFD simulations.
3. The developed machine learning model enables real-time predictions of 3D LVF distributions under various injection pressures and fuel temperatures. The proposed ANN model reduces the need for extensive computational optimization time and minimizes costs compared to CFD.
4. The machine learning model presented in this study can be adapted to various fuel types and operating conditions and can serve as a versatile spray model. It can also help overcome challenges related to cold start emissions.

Author Contributions: Conceptualization, Methodology, Investigation, Writing—original draft, Y.E.M.; data curation, K.L.; Supervision, Validation, Writing—review & editing, J.H. All authors have read and agreed to the published version of the manuscript.

Funding: This research received no external funding.

Data Availability Statement: Data will be made available on request.

Conflicts of Interest: The authors declare no conflict of interest.

References

1. Patrick, M. December 2023 Market Beat. Available online: https://www.nada.org/media/9244/download (accessed on 28 September 2024).
2. NOAA Research. Record Carbon Dioxide Emissions Impeding Progress on Meeting Climate Goals. Available online: https://research.noaa.gov/2023/12/05/record-fossil-carbon-dioxide-emissions-impeding-progress-on-meeting-climate-goals-report/#:~:text=Greenhouse%20gas%20emissions%20from%20fossil,by%20the%20Global%20Carbon%20Project (accessed on 20 February 2024).
3. Wen, M.; Zhang, C.; Yue, Z.; Liu, X.; Yang, Y.; Dong, F.; Liu, H.; Yao, M. Effects of Gasoline Octane Number on Fuel Consumption and Emissions in Two Vehicles Equipped with GDI and PFI Spark-Ignition Engine. *J. Energy Eng.* **2020**, *146*, 04020069. [CrossRef]
4. El Marnissi, Y.; Hwang, J. Microscopic Imaging on Diesel Spray and Atomization Process. *Processes* **2024**, *12*, 359. [CrossRef]
5. He, X.; Xu, K.; Xu, Y.; Zhang, Z.; Wei, W. Effects of nozzle diameter on the characteristic time scales of diesel spray two-stage ignition under cold-start conditions. *Fuel* **2023**, *335*, 126700. [CrossRef]
6. Shi, Z.; Lee, C.F.; Wu, H.; Wu, Y.; Zhang, L.; Liu, F. Optical diagnostics of low-temperature ignition and combustion characteristics of diesel/kerosene blends under cold-start conditions. *Appl. Energy* **2019**, *251*, 113307. [CrossRef]
7. Tong, K.; Quay, B.; Zello, J.; Santavicca, D. *Fuel Volatility Effects on Mixture Preparation and Performance in a GDI Engine During Cold Start*; SAE Technical Paper 2001-01-3650; SAE International: Warrendale, PA, USA, 2001. [CrossRef]
8. Lien, H.P.; Li, Y.; Pati, A.; Sadiki, A.; Hasse, C. Numerical studies of gasoline direct-injection sprays (ECN Spray G) under early- and late-injection conditions using Large Eddy Simulation and droplets-statistics-based Eulerian–Lagrangian framework. *Fuel* **2024**, *357*, 129708. [CrossRef]
9. Piazzullo, D.; Costa, M.; Allocca, L.; Montanaro, A.; Rocco, V. A 3D CFD Simulation of GDI Sprays Accounting for Heat Transfer Effects on Wallfilm Formation. *Source SAE Int. J. Engines* **2017**, *10*, 2166–2175. [CrossRef]
10. Gerbino, F.; Tretola, G.; Morgan, R.; Atkins, P.; Vogiatzaki, K. Influence of the initial droplet distribution on the prediction of spray dynamics in Eulerian-Lagrangian simulations. *Int. J. Multiph. Flow* **2021**, *141*, 103642. [CrossRef]
11. Schmidt, D.; Maulik, R.; Lyras, K. Machine learning accelerated turbulence modeling of transient flashing jets. *Phys. Fluids* **2021**, *33*, 127104. [CrossRef]
12. Ravindran, A.C.; Kokjohn, S.L. Combining machine learning with 3D-CFD modeling for optimizing a DISI engine performance during cold-start. *Energy AI* **2021**, *5*, 100072. [CrossRef]
13. Richards, B.; Emekwuru, N. Using Machine Learning to Predict Synthetic Fuel Spray Penetration from Limited Experimental Data Without Computational Fluid Dynamics. In Proceedings of the International Conference on Energy and Sustainable Futures, Dubai, United Arab Emirates, 5–6 December 2023; pp. 51–59. [CrossRef]
14. Laget, O.; Pacaud, P.; Perrin, H. Démarrage à froid d'un moteur Diesel à bas taux de compression: Investigations expérimentales et numériques RANS tridimensionnelles. *Oil Gas Sci. Technol.* **2009**, *64*, 407–429. [CrossRef]
15. Thuerey, N.; Weißenow, K.; Prantl, L.; Hu, X. Deep learning methods for reynolds-averaged navier–stokes simulations of airfoil flows. *AIAA J.* **2020**, *58*, 25–36. [CrossRef]
16. Paredi, D.; Lucchini, T.; D'Errico, G.; Onorati, A.; Pickett, L.; Lacey, J. Validation of a comprehensive computational fluid dynamics methodology to predict the direct injection process of gasoline sprays using Spray G experimental data. *Int. J. Engine Res.* **2020**, *21*, 199–216. [CrossRef]
17. Zhang, Y.; Xu, S.; Zhong, S.; Bai, X.S.; Wang, H.; Yao, M. Large eddy simulation of spray combustion using flamelet generated manifolds combined with artificial neural networks. *Energy AI* **2020**, *2*, 100021. [CrossRef]
18. Es-Sahli, O.; Sescu, A.; Afsar, M.Z.; Buxton, O.R.H. Investigation of wakes generated by fractal plates in the compressible flow regime using large-eddy simulations. *Phys. Fluids* **2020**, *32*, 105106. [CrossRef]
19. Hwang, J.; Lee, P.; Mun, S.; Karathanassis, I.K.; Koukouvinis, F.; Tagliante, F.; Nguyen, T.; Pickett, L. A New Pathway for Prediction of Gasoline Sprays using Machine-Learning Algorithms. *SAE Int. J. Adv. Curr. Pract. Mobil.* **2022**, *5*, 343–356. [CrossRef]
20. Chang, M.; Park, S. Predictions and analysis of flash boiling spray characteristics of gasoline direct injection injectors based on optimized machine learning algorithm. *Energy* **2023**, *262*, 125304. [CrossRef]
21. Tian, J.; Liu, Y.; Bi, H.; Li, F.; Bao, L.; Han, K.; Zhou, W.; Ni, Z.; Lin, Q. Experimental study on the spray characteristics of octanol diesel and prediction of spray tip penetration by ANN model. *Energy* **2022**, *239*, 121920. [CrossRef]
22. Hwang, J.; Lee, P.; Mun, S.; Karathanassis, I.K.; Koukouvinis, P.; Pickett, L.M.; Gavaises, M. Machine-learning enabled prediction of 3D spray under engine combustion network spray G conditions. *Fuel* **2021**, *293*, 120444. [CrossRef]
23. Thangaraja, J.; Zigan, L.; Rajkumar, S. A machine learning framework for evaluating the biodiesel properties for accurate modeling of spray and combustion processes. *Fuel* **2023**, *334*, 126573. [CrossRef]
24. Seo, J.; Yun, B.; Kim, J.; Shin, M.; Park, S. Development of a cold-start emission model for diesel vehicles using an artificial neural network trained with real-world driving data. *Sci. Total Environ.* **2022**, *806*, 151347. [CrossRef]
25. Giannelli, R.A.; Stubleski, R.; Saunders, A. Semi-empirical Analysis of Cold Start Emissions. *Int. J. Fuels Lubr.* **2014**, *7*, 591–599. [CrossRef]
26. Sabatini, S.; Kil, I.; Dekar, J.; Hamilton, T.; Wuttke, J.; Smith, M.A.; Hoffman, M.A.; Onori, S. A new semi-empirical temperature model for the three way catalytic converter. *IFAC-PapersOnLine* **2015**, *48*, 434–440. [CrossRef]
27. Settles, G.S. *Schlieren and Shadowgraph Techniques*; Springer: Berlin/Heidelberg, Germany, 2001.

28. Payri, R.; Salvador, F.J.; Bracho, G.; Viera, A. Differences between single and double-pass schlieren imaging on diesel vapor spray characteristics. *Appl. Therm. Eng.* **2017**, *125*, 220–231. [CrossRef]
29. Sada, A.; Kinoshita, Y.; Shiota, S.; Kiya, H. Histogram-Based Image Pre-processing for Machine Learning. In Proceedings of the 2018 IEEE 7th Global Conference on Consumer Electronics, Nara, Japan, 9–12 October 2018.
30. Jourdain, C.; Weiss, J.; Seers, P. Comparison of image preprocessing methods for fuel droplet characterization. In Proceedings of the 47th AIAA Thermophysics Conference, Denver, CO, USA, 5–9 June 2017; American Institute of Aeronautics and Astronautics Inc. (AIAA): Reston, VA, USA, 2017. [CrossRef]
31. Available online: http://www.philiplaven.com/mieplot.htm (accessed on 10 October 2024).
32. Badra, J.; Sim, J.; Pei, Y.; Viollet, Y.; Pal, P.; Futterer, C.; Brenner, M.; Som, S.; Farooq, A.; Chang, J. Combustion System Optimization of a Light-Duty GCI Engine Using CFD and Machine Learning. *SAE Tech. Pap.* **2020**. [CrossRef]
33. Kochkov, D.; Smith, J.A.; Alieva, A.; Wang, Q.; Brenner, M.P.; Hoyer, S. Machine learning-accelerated computational fluid dynamics. *Proc. Natl. Acad. Sci. USA* **2021**, *118*, e2101784118. [CrossRef] [PubMed]
34. Aleiferis, P.G.; Shukla, J.; Brewer, M.; Cracknell, R.F. Spray development of iso-octane, ethanol, hydrous ethanol and water from a multi-hole injector under ultra cold fuel temperature conditions. *Fuel* **2021**, *303*, 120983. [CrossRef]
35. Hemdal, S.; Denbratt, I.; Wärnberg, J. Stratified Cold Start Sprays of Gasoline-Ethanol Blends. *Int. J. Fuels Lubr.* **2009**, *2*, 683–696. [CrossRef]
36. Lee, K.; Pintor, D.L.; Assanis, D.; Cho, S.; Hwang, J. Fuel temperature and injection pressure influence on the cold start GDI sprays. *Appl. Energy Combust. Sci.* **2023**, *16*, 100206. [CrossRef]
37. Kook, S.; Pickett, L.M. Liquid length and vapor penetration of conventional, Fischer-Tropsch, coal-derived, and surrogate fuel sprays at high-temperature and high-pressure ambient conditions. *Fuel* **2012**, *93*, 539–548. [CrossRef]
38. Lehnert, B.; Weiss, L.; Berrocal, E.; Wensing, M. Quantifying extinction imaging of fuel sprays considering scattering errors. *Int. J. Engine Res.* **2023**, *24*, 4413–4420. [CrossRef]